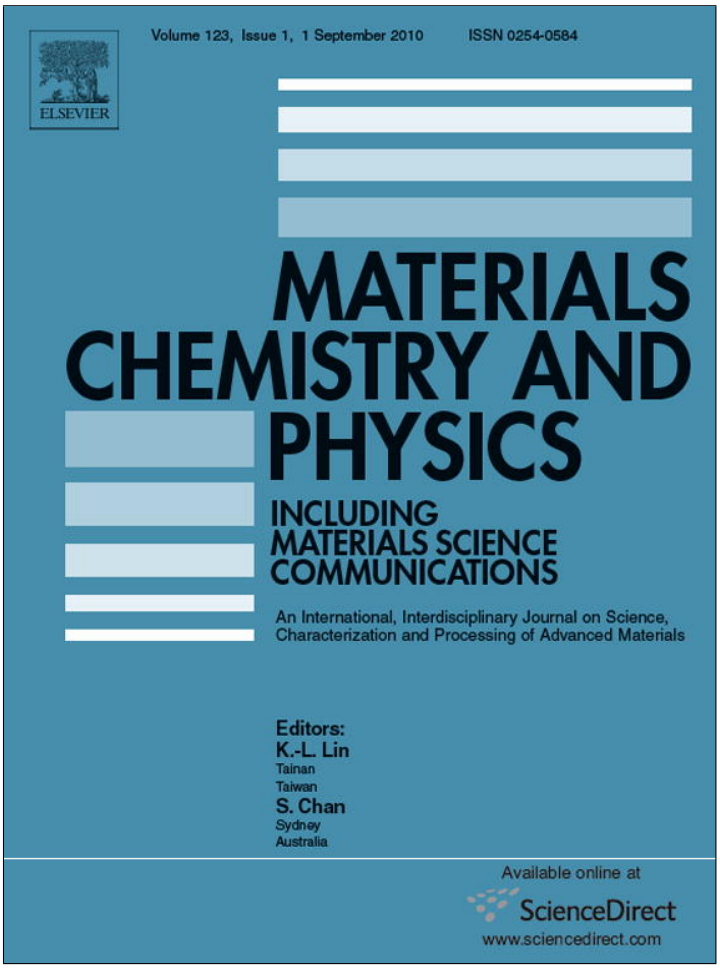

Materials Chemistry and Physics 123 (2010) 191–198

Contents lists available at ScienceDirect

Materials Chemistry and Physics

journal homepage: www.elsevier.com/locate/matchemphys

The Morin transition in nanostructured pseudocubic hematite: Effect of the intercrystallite magnetic exchange

J.F. Bengoa [a], A.M. Alvarez [a], A.E. Bianchi [b], G. Punte [b], R.E. Vandenberghe [c], R.C. Mercader [b], S.G. Marchetti [a,*]

[a] Departamento de Química, Facultad de Ciencias Exactas, Universidad Nacional de La Plata, CCT-La Plata, CONICET, CINDECA, CICPBA, 47 No. 257, 1900 La Plata, Argentina
[b] Departamento de Física, IFLP-CONICET, CCT-La Plata, Facultad de Ciencias Exactas, Universidad Nacional de La Plata, CC. 67, 1900 La Plata, Argentina
[c] Department of Subatomic and Radiation Physics, Ghent University, Proeftuinstraat 86, B-9000 Ghent, Belgium

ARTICLE INFO

Article history:
Received 7 July 2009
Received in revised form 2 December 2009
Accepted 30 March 2010

Keywords:
Magnetic materials
Nanostructures
Mössbauer spectroscopy
Magnetic properties

ABSTRACT

The Morin transition in α-Fe_2O_3 particles with homogeneous pseudocubic morphology of about 1.8 μm side has been studied by different techniques. The particles are made up of nanometric crystallites with a narrow size distribution. Samples annealed at 673, 773 and 873 K, yielded Morin transition temperatures, T_M, of about 230, 241, and 245 K, respectively, which are lower than the bulk value, $T_M \approx 263$ K. In addition, the temperature range ΔT_M through which these samples undergo the transition is very narrow with respect to the values reported in the literature. Ranges of 20, 10 and 8 K, were obtained for the samples annealed at 673, 773 and 873 K. In this work, through the estimation of the exchange magnetic energy, we demonstrate that the existence of the Morin transition, and its shift and breadth are related to the presence of intercrystallite interactions within the pseudocubic particles. These intercrystallite interactions are modified by the annealing treatments, which help to remove non-stoichiometric hydroxyl groups and incorporated water molecules.

1. Introduction

The Morin transition in pure bulk hematite (α-Fe_2O_3) occurs at $T_M \approx 263$ K. Cooling through that temperature, the Fe^{3+} magnetic moments turn 90° from their antiparallel but slightly canted weak ferromagnetic (WF) arrangement in the basal plane of the hexagonal structure to a completely antiferromagnetic (AF) arrangement parallel to the *c*-axis. It is generally accepted in the literature that the Morin transition occurs because of the different thermal dependence of the single-ion and dipolar magnetic anisotropy terms [1]. However, the detailed dependence of the parameters that influence these terms is still a matter of discussion [2], particularly when the systems are made of nanoparticles [3].

Although much has been written about the causes and conditions that modify the Morin transition temperature or suppress it for different kinds of samples [4,5], the descriptions generally allude to empirical relationships between different parameters, like the volume expansion or inhomogeneous dilation of the cell parameters with hydroxyls or structural water molecules [6]. To our knowledge, the results have not been related yet to the physical causes that influence directly the change of the starting and ending temperatures of the Morin transition.

In this work, through careful measurements by several techniques, we have been able to establish a connection between the exchange magnetic energy – produce by interparticle interactions in physical contact – and the nature of the Morin transition in nanostructured α-Fe_2O_3 particles with narrow crystallite size distribution and homogeneous pseudocubic morphology.

2. Experimental

Pseudocubic α-Fe_2O_3 particles were synthesized by a hydrothermal route following, with minor changes, the methodology proposed by Sugimoto et al. [7]. 100 cm^3 of NaOH solution (5.4 M) were added to 100 cm^3 of well-stirred $FeCl_3$ solution (2.0 M) for 5 min. The stirring was continued over 10 min. The gel was kept at 373 K for 12 days into a tight container. Finally, the product was washed and centrifuged several times to eliminate all the existing NaCl, and overnight dried in air at 353 K.

We call this compound *as-prepared hematite* (Hap). The sample was divided into five batches that were annealed at five different temperatures, namely, 473, 573, 673, 773 and 873 K for 12 h in a flow of 150 cm^3 min^{-1} of synthetic dry air. In this way, we obtained the solids named H473, H573, H673, H773 and H873, respectively.

The materials were characterized by X-ray diffraction (XRD), scanning electron microscopy (SEM), graphite furnace atomic absorption spectroscopy, N_2 physisorption measurements (BET), thermal gravimetric analysis (TGA), Fourier transform infrared spectroscopy (FT-IR), Mössbauer spectroscopy (MS) and AC susceptibility.

All XRD patterns were measured using a standard automated powder X-ray diffraction system Philips PW 1710 with diffracted-beam graphite monochromator using Cu Kα radiation (λ = 1.5406 Å). Data were taken between 2θ = 20 and 70° with steps of 0.02° and counting time of 2 s per step. The instrumental peak profile was obtained taking as reference a very pure hematite sample (Cerac Inc., 100 mesh, 99.995%, wt/wt) annealed at 1273 K during 24 h in dry air flow. All patterns

* Corresponding author.
E-mail address: march@quimica.unlp.edu.ar (S.G. Marchetti).

0254-0584/$ – see front matter © 2010 Elsevier B.V. All rights reserved.
doi:10.1016/j.matchemphys.2010.03.081

were analyzed by the Rietveld method, using a modified pseudo Voigt function, considering anisotropic size and strain line broadening. The shape anisotropy of the crystallites was analyzed through the phenomenological model of Järvinen [8], while strain anisotropy was taken into account using Stephen's model [9]. These approximations were employed as implemented in the FullProf suite package [10].

The microphotographs were obtained with a Phillips 505 scanning electron microscope according to the normal procedures.

The atomic absorption spectroscopy assays were carried out with a Varian AA240, the BET measurements were realized with a Micromeritics ASAP 2020 analyzer, and the TGA measurements were carried out with a Shimadzu TGA-50 system.

The FT-IR absorption spectra were acquired with a Bruker IFS66 spectrometer with 1 cm^{-1} resolution by co-addition of 32 scans. The samples were prepared as potassium bromide discs, in a 1:100 proportion.

The Mössbauer spectra were recorded with a standard 512 channels spectrometer in transmission geometry. Low temperature measurements were performed in a helium closed-cycle refrigerator at temperatures ranging from 15 to 298 K and at 4.2 K in a liquid He bath cryostat. The source was of ^{57}Co in a Rh matrix, of 50 mCi nominal activity. The velocity calibration was performed against a 12 μm thick α-Fe foil at room temperature. The spectra were fitted to lines of Lorentzian shape (with equal widths for each component of the spectrum) using a least-squares non-linear computer fitting program with constrains.

The AC susceptibility measurements were taken between 13 and 325 K in a LakeShore 7130 susceptometer in zero DC field using an exciting field of 1 Oe amplitude and a frequency of 825 Hz.

3. Results and discussion

Elemental analyses by atomic absorption spectroscopy indicate that all samples contain only iron and oxygen, and a maximum Na content, as impurity, of 920 ppm.

Fig. 1a and b display the SEM micrographs of Hap and H873. The Hap sample consists of uniform-sized particles of 1.8 ± 0.2 μm side with pseudocubic morphology in coincidence with the results of Sugimoto et al. [7]. The different annealing treatments did not produce morphological or size changes in the particles, as demonstrated by the H873 SEM micrograph. The particle size for this sample is 1.9 ± 0.1 μm side. These sizes were determined by a statistical counting using the SEM micrographs.

The XRD results (Fig. 2) show that the only compound in the samples is α-Fe_2O_3 for all the investigated specimens. Since the particles are pseudo cubes with an average side of about 1.8 μm and the diffraction lines show considerable broadening, we conclude that all the samples are polycrystalline. The same results have been reported also by Shindo et al. [11] and Rath et al. [12].

The Mössbauer parameters of all samples correspond to pure α-Fe_2O_3. This is coherent with the XRD results. As an example, Table 1 displays the results obtained for Hap. Its hyperfine parameters are in agreement with Vandenberghe et al. [13]. In addition, it can be seen that in this sample the Morin transition is completely suppressed, resulting in a single WF phase down to 4.2 K. This is evidenced by its quadrupole shift, 2ε, which does not change its sign over all the temperature range.

In order to study the Morin transition through the magnetic behavior we measured the Mössbauer spectra and the AC susceptibility of all samples in the temperature range between 298 and 4.2 K.

Table 1
Mössbauer parameters of Hap at 298 and 4.2 K.

	Species	Parameters
α-Fe_2O_3 (WF) 298 K	H (T)	51.20 ± 0.02
	δ (mm s^{-1})	0.372 ± 0.002
	2ε (mm s^{-1})	−0.211 ± 0.005
α-Fe_2O_3 (AF) K	H (T)	53.55 ± 0.01
	δ (mm s^{-1})	0.475 ± 0.002
	2ε (mm s^{-1})	−0.110 ± 0.003

WF: weak ferromagnetic phase; AF: antiferromagnetic phase; H: hyperfine magnetic field in Tesla; δ: isomer shift (all the isomer shifts are referred to α-Fe at 298 K); 2ε: quadrupole shift.

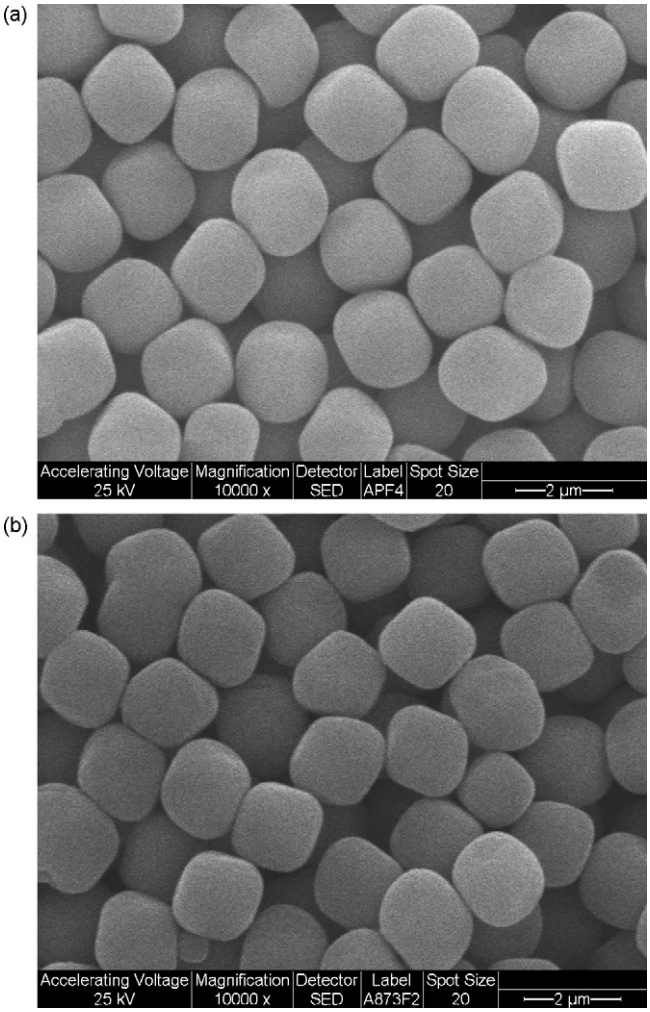

Fig. 1. (a) Scanning electron micrograph of Hap (10,000×). (b) Scanning electron micrograph of H873 (10,000×).

The Mössbauer spectra of Hap, H473 and H573 did not show the Morin transition down to 4.2 K. Instead, for H673, H773 and H873 samples, a clear Morin transition is evidenced in the Mössbauer spectra by the thermal dependence of their quadrupole shift (Fig. 3) and hyperfine field (not shown). The transition region ΔT_M at which both arrangements AF and WF coexist spans a range, which is extremely narrow in comparison with other small-crystallites of hematite of similar size [4,14] (Table 2). This is evidence that the pseudocubic particles have a very narrow distribution of crystallite sizes. An increase of T_M and a decrease of ΔT_M are observed when the annealing temperature is higher. As an example, Fig. 4 exhibits the spectra sequence obtained for H673 at some representative temperatures.

Fig. 5 displays the AC susceptibility results. The $\chi'(T)$ curves of the samples annealed at temperatures below 573 K are smooth for the whole temperature range, indicating that the Morin transition has been suppressed for those samples. Instead, when the annealing temperature is higher, a significant drop in the $\chi'(T)$ dependence is apparent when the samples are cooled through the Morin transition temperature, denoting that the transition has taken place (with different ΔT_M for each sample). When the samples are annealed at higher temperatures, the range over which the fall in $\chi'(T)$ takes place gets narrower and T_M approaches the bulk value. Table 2 displays the values of T_M and ΔT_M obtained by AC susceptibility which follow the same trend as those yielded by the Mössbauer results. The values yielded by both

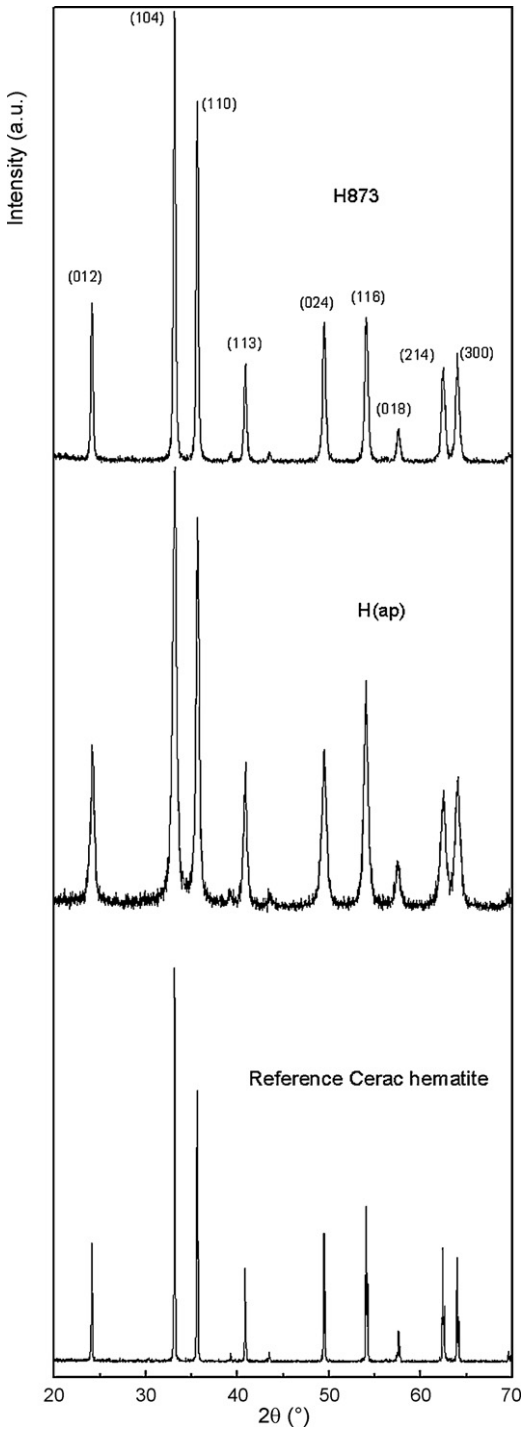

Fig. 2. XRD patterns of Hap and H873 samples and pure hematite (annealed at 1273 K during 24 h in dry air flow) used as reference.

techniques are not coincident because of their different sampling times.

In order to interpret this magnetic behavior we carried out a detailed study of all samples using XRD, TGA and IR.

The Rietveld fits of XRD patterns assuming an isotropic microstructure were not satisfactory. In addition, a comparison of the line widths shows that the breadth is not a smooth function of the diffraction angle. Consequently, shape and strain anisotropy parameters were included in the Rietveld analyses. Table 3 shows the resulting lattice parameters, "*a*" and "*c*", cell volumes, *V*, size of the coherently diffracting domains, $\langle D \rangle$ (apparent average size of the crystallites), maximum strain parameter, $\langle \varepsilon \rangle$, and the four Fe–O–Fe angles, which take part in the super-exchange pathways between the two magnetically nonequivalent Fe atoms contained in the primitive cell. It is important to remark that our results show an isotropic contraction of the cell volume with the annealing temperature. This trend is opposite to the results of Dang et al. [6] who found an expansion of the cell volume that is anisotropic; "*a*" increases while "*c*" decreases. We believe that this difference may have its origin in the presence of the important loading of $SO_4^=$ groups that Dang et al. [6] report for their samples, while in ours we did not find any significant leftover from reactants used during the preparation steps.

The values in Table 3 demonstrate that the average crystallite diameter remains constant up to 573 K. However, when the annealing temperature reaches 673 K, an apparent sintering takes place by which at 873 K the crystallite sizes reach about four times the original ones. According to the results and the model proposed by Dang et al. [6] the samples H673, H773 and H873 lie in a region of the "*c*" versus "*a*" plot (Fig. 6) in which the Morin transition is observed. The cell parameters of our Hap, H473 and H573 samples belong to the same region of the plot of Fig. 6 but do not exhibit the Morin transition. This is expected since the size of the coherently diffracting domains of these samples is smaller than 20 nm. Therefore, the model proposed by Dang et al. [6] cannot explain our results.

On the other hand, the values of maximum strain and super-exchange angles remain nearly constant for annealing temperatures up to H873. Therefore, it is reasonable to assume that the entailing small changes of the super-exchange coupling are not large enough to change the configuration of the magnetic moments from the weak ferromagnetic state to the AFM state with a dramatic reorientation of the magnetic moments of the two sublattice sites.

We must seek a different origin to explain the different magnetic behavior of the samples. One possibility is that the changes be related to the loss of water molecules and non-stoichiometric hydroxyls, and to the healing of vacancies. These changes are apparent in the results yielded by the TGA and FT-IR studies.

The TGA derivatives are reported in Fig. 7. The sample Hap loses 3.65% of its weight when heated up to 1173 K. The 90% of this loss occurs continuously up to about 743 K. The weight loss rate is higher at 328 K. Considering that H473 was subjected to a previous calcination at 473 K before the TGA assay, and that Hap had already lost 1.95% of its weight up to 473 K, it was expected that H473 should have lost only 1.70% of weight. However, the total experimental value found was 3.61%, which leads us to think that very likely

Table 2
Morin transition results from Mössbauer and susceptibility data. T_M is the Morin temperature and ΔT_M is the temperature range over which the transition occurs.

Samples	T_M from MS (K)	ΔT_M from MS (K)	T_M from AC susceptibility (K)	ΔT_M from AC susceptibility (K)
Hap	–	–	–	–
H473	–	–	–	–
H573	–	–	–	–
H673	230 ± 5	20 ± 4	232 ± 2	36 ± 5
H773	241 ± 4	10 ± 3	252 ± 2	18 ± 3
H873	245 ± 4	8 ± 4	257 ± 2	12 ± 2

Table 3
Hexagonal cell parameters (a and c), volume size (V), apparent crystallite size $\langle D\rangle$, maximum strain $\langle\varepsilon\rangle$ and super-exchange interaction angles. The numbers within parentheses are the estimated errors in the least significant figures except for $\langle D\rangle$ and $\langle\varepsilon\rangle$, in which they are a measure of the degree of anisotropy. The subindexes identify the atoms in the same way as the nomenclature used by Blake[a].

	Samples					
	Hap	H473	H573	H673	H773	H873
a (Å)	5.0387 (1)	5.0374 (1)	5.0372 (1)	5.0358 (1)	5.0356 (1)	5.0356 (1)
c (Å)	13.7871 (1)	13.7670 (1)	13.7660 (1)	13.7541 (1)	13.7518 (1)	13.7515 (1)
V (Å^3)	303.13 (1)	302.54 (1)	302.49 (1)	302.06 (1)	301.98 (1)	301.98 (1)
$\langle D\rangle$ (nm)	16.8 (1.8)	16.6 (2.6)	17.0 (2.8)	22.9 (4.8)	31.3 (7.1)	52.6 (11.8)
$\langle\varepsilon\rangle$ ($\times 10^{-4}$)	26.1 (5.9)	30.9 (7.7)	30.8 (7.1)	24.3 (1.9)	24.6 (2.8)	27.0 (3.4)
Fe_1–O_3–Fe_2 (°)	93.82 (4)	93.87 (4)	93.88 (4)	94.16 (4)	94.28 (4)	94.10 (4)
Fe_6–O_4–Fe_7 (°)	86.26 (8)	86.27 (8)	86.20 (8)	87.46 (8)	87.69 (6)	87.14 (8)
Fe_2–O_7–Fe_6 (°)	131.65 (7)	131.64 (7)	131.63 (7)	132.04 (7)	132.13 (7)	131.88 (7)
Fe_1–O_1–Fe_6 (°)	119.87 (6)	119.82 (6)	119.83 (6)	118.21 (6)	117.89 (6)	118.67 (6)

[a] R.L. Blake, R.E. Hessevick, T. Zoltai and L.W. Finger, The Am. Mineralogist, 51, 123 (1966).

the sample H473 has re-adsorbed atmospheric water after the calcination treatment. A very similar behavior was found for H573. Instead, H673, H773 and H873 did not experience the re-adsorption of water. An explanation for this result is that the sintering process, which begins at temperatures between 573 and 673 K, according to the XRD analyses, would lead to the disappearance of intercrystallite spaces, where the water molecules may be adsorbed. This conclusion is coherent with the BET specific surface area decrease from 29 for Hap to 6 $m^2\ g^{-1}$ for H873.

On the other hand, in all annealed samples, we have detected two other maxima corresponding to minor steps of the weight loss, namely, at about 573–613 K and around 903–963 K. According to Dang et al. [6] the loss of incorporated H_2O is effective up to 473 K and the loss of structural OH groups (non-stoichiometric hydroxyls) and their associated cationic vacancies can be detected up to 1273 K [15]. The non-stoichiometric hydroxyls appear when these groups occupy $O^{=}$ positions within the hematite structure, associated with vacancies of Fe^{3+} in the lattice [16]. In our samples, the two steps mentioned above would correspond to the removal of these OH groups and to the healing of vacancies. Consequently, using the TGA values and the general structural formula given by Dang et al. [6], $Fe_{(2-x/3)}O_{(3-x)}(OH)_x$, we can suggest the stoichiometry for all samples that is shown in Table 4. In the nomenclature proposed by Dang et al. [6], Hap, H473 and H573 are samples of proto-hydrohematite and the other three samples are of hydro-hematite.

To investigate the existence of the OH groups we used the FT-IR technique. Because of the way in which the spectra were obtained, all of them can be compared only qualitatively. All samples displayed two bands (zone not shown) centered at 482 and 569 cm^{-1} assignable to the stretching vibrations of Fe–O characteristic of hematite [17]. Besides, Fig. 8 exhibits for all samples a broad band centered at about 3430 cm^{-1}, generally attributed to the stretching of non-stoichiometric hydroxyls [17]. The presence of these groups detected by FT-IR after annealing at high temperatures, even at 873 K, is coherent with the TGA results.

The water and OH loss, detected by TGA and FT-IR, produces intra-particle changes but does not alter the particle size and morphology (as is evidenced by SEM) and does not modify substantially the crystallite structure (as is shown by XRD results). The sintering process of the crystallites leads to an increase in their physical contact, diminishing the number of channels filled with adsorbed water (as is revealed by BET measurements).

In order to analyze the correlation between the above structural changes and the magnetic behavior, we will describe some aspects of the anisotropy for rotation of the magnetization sublattices out of the (1 1 1) plane and within this plane. The effective anisotropy constant, κ, for this process is given by [18]:

$$\frac{1}{\kappa} = \frac{1}{2K_{BU}} + \frac{1}{2\left|K_1\right|} \tag{1}$$

where K_1 and K_{BU} are the anisotropy constants for rotation of the magnetization sublattices out of the (1 1 1) plane and within this plane, respectively.

For bulk hematite, the temperature variation of K_1 is generally modeled using mean-field theory [1]. In this theory, K_1 is a nearly constant positive value for temperatures below about 150 K. At higher temperatures, it decreases almost linearly with temper-

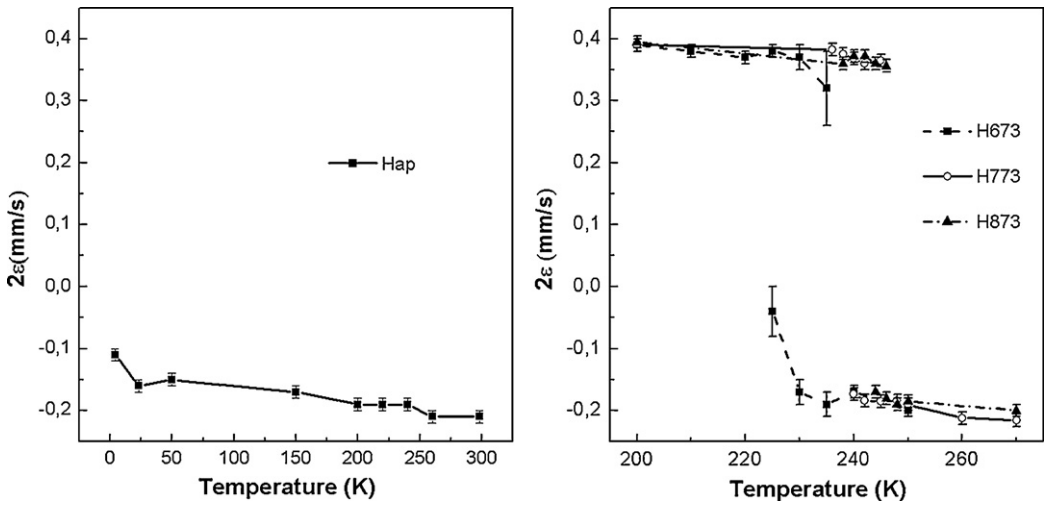

Fig. 3. Thermal dependence of the quadrupole shift (2ε) for Hap, H673, H773 and H873.

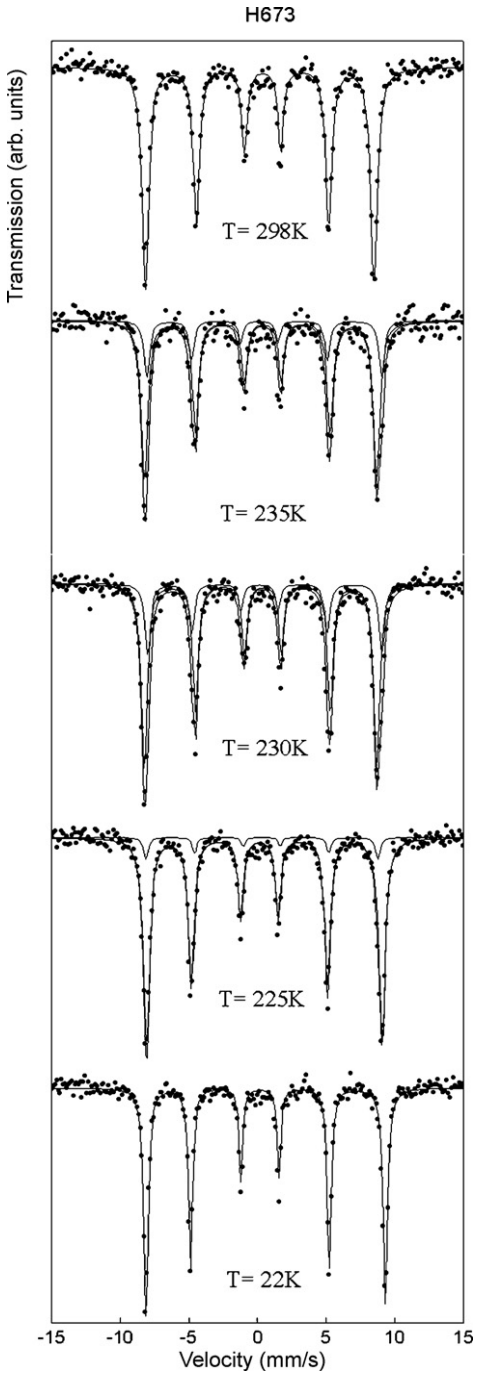

Fig. 4. Mössbauer spectra of H673 at some representative temperatures.

ature up to about 500 K. The K_1 constant changes its sign from positive to negative at the Morin transition temperature, T_M. For nanoparticles it is known that T_M is smaller than the bulk value and the Morin transition is absent at least down to 5 K for particles

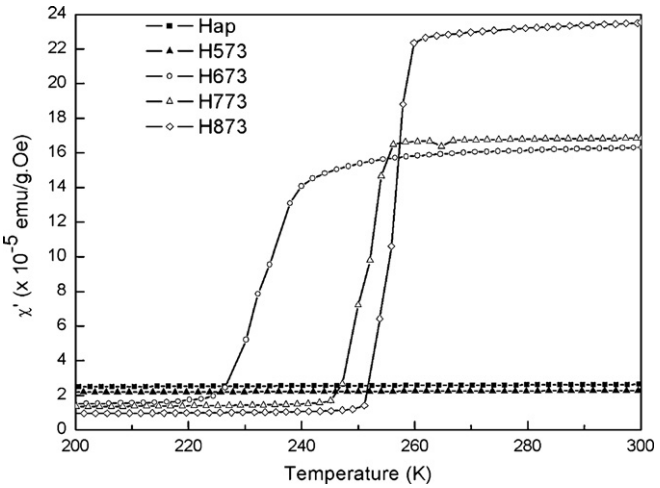

Fig. 5. In-phase AC susceptibility results, measured with a frequency of 825 Hz and amplitude of 1 Oe.

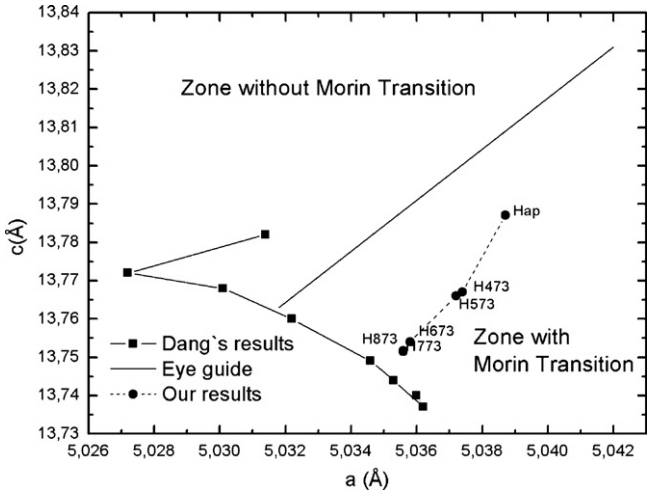

Fig. 6. Current results positions in the Dang et al. plot [6]. The lines are guides for the eye.

smaller than about 20 nm [1,19–21]. In Ref. [22] for 16 nm hematite nanoparticles it was shown that $-K_1$ was so large that the sublattice magnetization vectors could be considered as confined to the (1 1 1) plane and hence that the $|K_1|^{-1}$ contribution to Eq. (1) could be neglected.

The angle θ between the sublattice magnetization directions and the [0 0 1] axis of α-Fe_2O_3 can be deduced from the quadrupole shift, 2ε, obtained from the Mössbauer spectra using the following equation:

$$2\varepsilon = \varepsilon_0(3\cos^2\theta - 1) \quad (2)$$

where $\varepsilon_0 = 0.200\ \text{mm s}^{-1}$. Therefore, if $-K_1$ is very large, the sublattice magnetization remains in the basal plane, $\theta = 90^\circ$ and $2\varepsilon = -0.200\ \text{mm s}^{-1}$ for all temperatures.

Table 4
Thermogravimetric results and stoichiometric formulae.

Samples	Total weight loss (%) (±0.01)	Weight lost at temperatures higher than 523 K (%) (±0.01)	Stoichiometric formula
Hap	3.65	1.33	$Fe_{1.957}O_{2.870}(OH)_{0.130}$ $(0.213{\cdot}H_2O)$
H473	3.61	1.31	$Fe_{1.957}O_{2.872}(OH)_{0.127}$ $(0.212{\cdot}H_2O)$
H573	2.25	0.94	$Fe_{1.970}O_{2.911}(OH)_{0.089}$ $(0.116{\cdot}H_2O)$
H673	0.35	0.34	$Fe_{1.989}O_{2.968}(OH)_{0.032}$
H773	0.20	0.17	$Fe_{1.995}O_{2.984}(OH)_{0.016}$
H873	0.06	0.06	$Fe_{1.998}O_{2.994}(OH)_{0.006}$

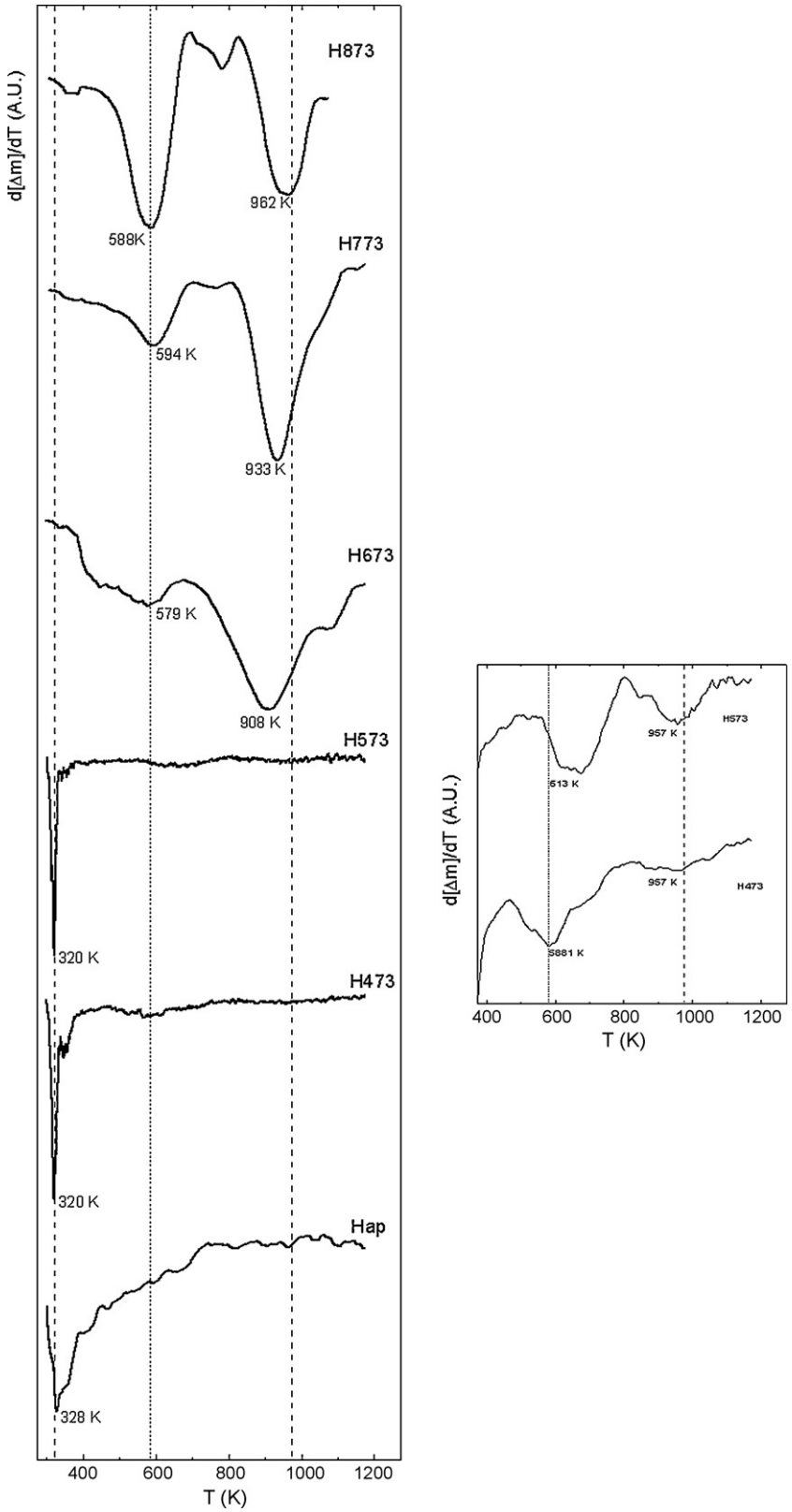

Fig. 7. TGA derivatives of all samples. For H473 and H573, the derivative scale was expanded for better understanding.

In our samples Hap, H473 and H573, which do not display any Morin transition, the 2ε values are very similar between them but different from $-0.200\,\mathrm{mm\,s^{-1}}$. As an example, $2\varepsilon = -0.110 \pm 0.003\,\mathrm{mm\,s^{-1}}$ (Table 1) for Hap at 4.2 K. From Eq. (2), the θ angle in this sample is 67°, indicating a sublattice magnetization out of the basal plane of 23°. This result is in agreement with that found by Frandsen and Mørup [23] for interacting α-Fe_2O_3 nanoparticles of 8 nm. These authors showed that the interparticle magnetic exchange interaction is a mechanism than can lead to the rotation of the sublattice magnetization away from the direc-

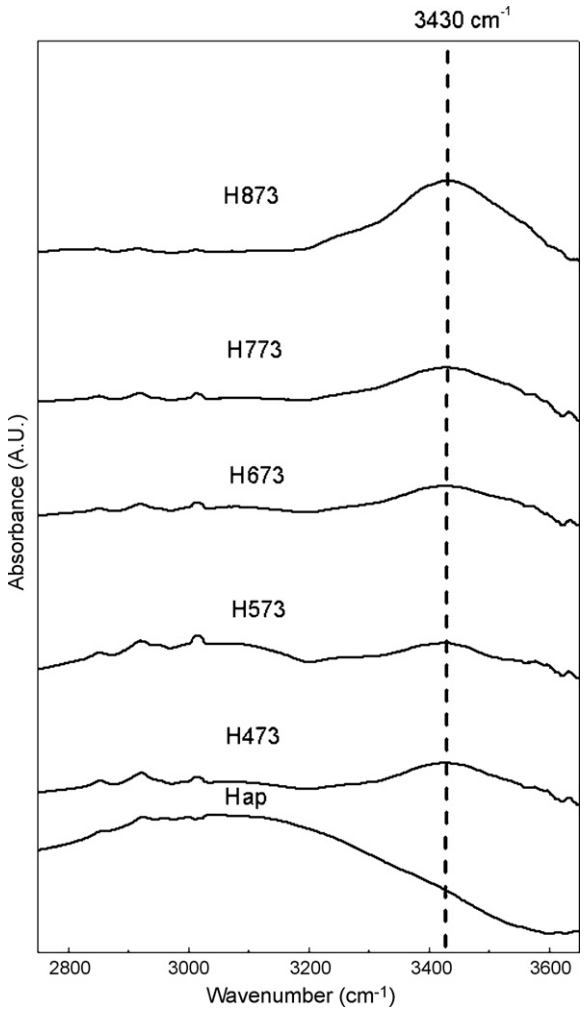

Fig. 8. IR spectra of all samples in 2750 and 3650 cm^{-1} range.

tion defined by the magnetic anisotropy. They estimated the net interaction magnetic energy (E_{int}) due to the exchange coupling between particles from:

$$E_{int} = -2K_1 V \cos\theta \quad (3)$$

where V is the crystallite volume.

The E_{int} estimated from Eq. (3) for Hap with a crystallite size of about 20 nm (Table 3), is of 2.6×10^{-20} J ($E_{int}/k = 1873$ K). This energy was calculated using the K_1 value estimated by Hansen et al. [18] for α-Fe_2O_3 nanoparticles of 20 nm, $K_1 = -7900\ J\,m^{-3}$. These authors assumed that the exchange coupling between neighboring crystallites is similar to that produced by super-exchange coupling between the iron atoms in bulk hematite. The average exchange coupling constants (J/k) for super-exchange pathways are about −20 K. Consequently, the exchange energy for a pair of Fe^{3+} ions is about 125 K [18]. Therefore, if a crystallite is connected to neighboring crystallites via only about 15 exchange bridges [$(E_{int}/k)/125\ K \approx 15$], with the same exchange coupling constant as within the particles, it would be enough to cause the rotation of the sublattice magnetization 23° out of the basal plane. Likely, more pairs of atoms are involved in the exchange coupling and perhaps, most of these have a weaker exchange coupling constant [18].

In our series of samples, H673 is the first one with Morin transition. In this case, the angle is $\theta = 0°$ below 230 K, and therefore, from Eq. (3), we can estimate $E_{int} \approx 6.62 \times 10^{-20}$ J, i.e., $E_{int}/k \approx 4794$ K. Consequently, if there are about 40 exchange bridges between neighboring crystallites present, the exchange magnetic energy is enough to overcome the anisotropic energy barrier, forcing the sublattice magnetization along the [0 0 1] axis, enabling the Morin transition to take place. The above discussion is in agreement with the structural characterization results since, from the annealing temperature of 673 K upward, the water re-adsorption has stopped, indicating that the channels between the crystallites have disappeared, increasing the number of contact points or "bridges" between them.

When the annealing temperature is increased beyond 673 K, the crystallites begin to sinter. Both effects, the channels disappearance and the sintering, are evidenced by the specific surface area decrease and the crystallite diameter increase. This last change produces a decrease of K_1 and, consequently, the Morin transition temperature increases and the transition region ΔT_M narrows.

4. Conclusions

Hematite prepared by wet synthesis is a complex system that undergoes drastic changes of its water and non-stoichiometric hydroxyl groups content with the annealing temperature. In the present work, we have demonstrated that the Morin transition is highly sensitive to the magnetic exchange energy between neighboring nanometric crystallites located inside the micrometric particles. Thus, when these crystallites remain practically isolated by means of channels with adsorbed water and with only a few contact points between them, the magnetic exchange energy produces a rotation of sublattice magnetizations of only 23° out of the basal plane. When the annealing temperature is about 673 K, the channels practically disappear, the contact points (or bridges) number between crystallites increases, the exchange magnetic energy increases dramatically and the Morin transition occurs. Annealing treatments at higher temperatures bring about an additional effect, the crystallite sintering that leads to an increase of the Morin temperature and a narrowing of the temperature range at which the Morin transition proceeds.

Finally, the present results demonstrate that to determine the global magnetic behavior in nanometric hematite crystallites it is necessary to consider simultaneously its size and the magnetic interactions between them.

Acknowledgments

The authors acknowledge partial economic support by CONICET (PIP 6524), ANPCyT (PICT 2005 38337 and PICT 2006 2315), *Comisión de Investigaciones Científicas de la Provincia de Buenos Aires* and *Universidad Nacional de La Plata*, Argentina. Part of this work was conducted within the agreement between FWO-Flanders and SECTIP-Argentina; project FW/PA/02-EIII/003. J.F.B. is member of CICPBA. A.M.A., G.P., R.C.M. and S.G.M. are members of CONICET. A.E.B. thanks UNLP for a research fellowship.

References

[1] A.H. Morrish, Canted Antiferromagnetism: Hematite, World Scientific, Singapore, 1994.
[2] F. Jiao, A. Harrison, J.C. Jumas, A.V. Chadwick, W. Kockelmann, P.G. Bruce, J. Am. Chem. Soc. 128 (2006) 5468.
[3] D.E. Madsen, S. Mørup, Phys. Rev. B 74 (2006) 014405.
[4] E. Van San, E. De Grave, R.E. Vandenberghe, H.O. Desseyn, L. Datas, V. Barron, A. Rousset, Phys. Chem. Miner. 28 (2001) 488.
[5] J.F. Bengoa, M.S. Moreno, S.G. Marchetti, R.E. Vandenberghe, R.C. Mercader, Hyperfine Interact. 161 (2005) 177.
[6] M.Z. Dang, D.G. Rancourt, J.E. Dutrizac, G. Lamarche, R. Provencher, Hyperfine Interact. 117 (1998) 271.
[7] T. Sugimoto, K. Sakata, A. Muramatsu, J. Colloid Interface Sci. 159 (1993) 372.
[8] M. Järvinen, J. Appl. Crystallogr. 26 (1993) 525.
[9] P.W. Stephens, J. Appl. Crystallogr. 32 (1999) 281.
[10] J. Rodríguez-Carvajal, Physica B 192 (1993) 55.

[11] D. Shindo, S. Aita, G. Park, T. Sugimoto, Mater. Trans. JIM 34 (1993) 1226.
[12] C. Rath, K.K. Sahu, S.D. Kulkarni, S. Anand, S.K. Date, R.P. Das, N.C. Mishra, Appl. Phys. Lett. 75 (1999) 4171.
[13] R.E. Vandenberghe, E. De Grave, C. Landuydt, L.H. Bowen, Hyperfine Interact. 53 (1990) 175.
[14] R.E. Vandenberghe, E. Van San, E. De Grave, G.M. da Costa, Czech. J. Phys. 51 (2001) 6639.
[15] E. Wolska, Zeits. für Kristall. 154 (1981) 69.
[16] D. Walter, Themochim. Acta 445 (2006) 195.
[17] H.D. Ruan, R.L. Frost, J.T. Kloprogge, L. Duong, Spectrochim. Acta A 58 (2002) 967.
[18] M.F. Hansen, S.B. Koch, S. Mørup, Phys. Rev. B 62 (2) (2000) 1124.
[19] W. Kündig, H. Bömmel, G. Constabaris, R.H. Lindquist, Phys. Rev. 142 (1966) 327.
[20] D. Schroer, R.C. Nininger Jr., Phys. Rev. Lett. 19 (1967) 632.
[21] R.C. Nininger Jr., D. Schroer, J. Phys. Chem. Solids 39 (1978) 137.
[22] F. Bødker, M.F. Hansen, C. Bender Koch, K. Lefmann, S. Mørup, Phys. Rev. B 61 (2000) 6826.
[23] C. Frandsen, S. Mørup, Phys. Rev. Lett. 94 (2005) 027202.